Zhou *et al. J Cancer Metastasis Treat.* 2025;11:25
DOI: 10.20517/2394-4722.2025.37

Journal of Cancer Metastasis and Treatment

Original Article

Open Access

Check for updates

Bioinformatics analysis and experimental validation of m^{3}C RNA methylation regulators in hepatocellular carcinoma: expression, function, and prognostic value

Wei Zhou[1], Junchao Lin[2], Yizhuo Wang[2], Aqiang Fan[1], Liu Hong[1], Xiaohua Li[1]

[1]Department of Digestive Surgery, Xijing Hospital of Digestive Diseases, Fourth Military Medical University, Xi'an 710032, Shaanxi, China.
[2]Xijing Hospital of Digestive Diseases, Fourth Military Medical University, Xi'an 710032, Shaanxi, China.

Correspondence to: Prof. Xiaohua Li and Prof. Liu Hong, Department of Digestive Surgery, Xijing Hospital of Digestive Diseases, Fourth Military Medical University, Xi'an 710032, Shaanxi, China. E-mail: xjyylixiaohua@163.com; hongliu180@126.com

How to cite this article: Zhou W, Lin J, Wang Y, Fan A, Hong L, Li X. Bioinformatics analysis and experimental validation of m^{3}C RNA methylation regulators in hepatocellular carcinoma: expression, function, and prognostic value. *J Cancer Metastasis Treat.* 2025;11:25. https://dx.doi.org/10.20517/2394-4722.2025.37

Received: 16 Mar 2025 **First Decision:** 9 Jul 2025 **Revised:** 27 Jul 2025 **Accepted:** 8 Sep 2025 **Published:** 29 Sep 2025

Academic Editor: Ciro Isidoro **Copy Editor:** Ping Zhang **Production Editor:** Ping Zhang

Abstract

Aim: Hepatocellular carcinoma (HCC) remains a major challenge due to poor prognosis. This study investigates 3-methylcytidine (m^{3}C) RNA methylation regulators to elucidate their roles in HCC and to develop a prognostic scoring system for clinical application.

Methods: We integrated data from 486 HCC patients [The Cancer Genome Atlas (TCGA) and Gene Expression Omnibus (GEO) datasets] and 16 pairs of clinical tissue samples. The expression, mutation profiles, and prognostic significance of 6 m^{3}C regulators were analyzed. Functional assays, including cell proliferation and migration, were performed, alongside immune infiltration analysis using single-sample gene set enrichment analysis (ssGSEA). Finally, an m^{3}C scoring system was constructed to evaluate prognostic potential.

Results: Most m^{3}C regulators (except METTL8) were upregulated in HCC tissues. Knockdown of METTL2, METTL6, ALKBH1, or ALKBH3, as well as overexpression of METTL8, inhibited HCC cell proliferation and migration. Two distinct m^{3}C modification modes were identified, each associated with unique clinical features. The m^{3}C score was positively correlated with longer overall survival in high-score patients and was associated with

© The Author(s) 2025. **Open Access** This article is licensed under a Creative Commons Attribution 4.0 International License (https://creativecommons.org/licenses/by/4.0/), which permits unrestricted use, sharing, adaptation, distribution and reproduction in any medium or format, for any purpose, even commercially, as long as you give appropriate credit to the original author(s) and the source, provide a link to the Creative Commons license, and indicate if changes were made.

tumor mutation burden (TMB) and expression of PD-1 and CTLA4, suggesting its potential to predict immunotherapy response.

Conclusion: This study highlights the genetic variation and prognostic relevance of m^3C methylation regulators in HCC and introduces a novel scoring system for prognosis prediction, providing a potential tool to guide HCC treatment strategies.

Keywords: Computational biology, RNA methylation, hepatocellular carcinoma, database, early diagnosis

INTRODUCTION

Primary liver cancer is one of the most common malignant tumors of the digestive system and ranks as the third leading cause of cancer-related deaths worldwide, posing a major global healthcare challenge[1,2]. Approximately 866,136 new liver cancer cases and 758,725 deaths occur annually worldwide[3], with hepatocellular carcinoma (HCC) being the predominant pathological subtype[4,5]. HCC is highly invasive and typically asymptomatic in its early stages; by the time clinical symptoms prompt diagnosis, the disease often progresses to an advanced stage, precluding the possibility of radical surgery[6-8]. Although advances in liver transplantation, minimally invasive resection, percutaneous ablation, radiotherapy, interventional therapy, systemic therapy, and immunotherapy have prolonged patient survival[9-13], the 5-year survival rate remains low, and overall prognosis remains poor. Thus, clarifying the pathogenesis of HCC is critical for developing new treatments and personalized medical strategies to improve patient outcomes and long-term survival.

HCC exhibits marked heterogeneity, and its genomic, epigenetic, and molecular expression profiles are critical for unraveling its pathogenesis[11-13]. With the continuous development of high-throughput sequencing technology, numerous RNA post-transcriptional modifications have been identified[14,15]. Transfer RNA (tRNA), one of the most abundant RNA species in cells, acts as a key adaptor in ribosome translation of the genetic code[16,17]. Among these modifications, 3-methylcytidine (m^3C) methylation occurs at specific tRNA positions: in the cytoplasm, it is present at position 32 of the anticodon loop of $tRNA^{Thr}$, $tRNA^{Ser}$, and $tRNA^{Arg}$, and at positions 20 or 47 of $tRNA^{Leu}$ and $tRNA^{Met-e}$[18]. This modification is essential for maintaining tRNA stability and biological function[19,20].

Notably, m^3C methylation differs from other well-studied RNA modifications such as N6-methyladenosine (m6A)-which primarily modulates mRNA splicing, export, and translation. By contrast, m^3C is predominantly enriched in tRNAs, where it enhances aminoacylation efficiency and ribosomal decoding fidelity. This unique tRNA targeting suggests that m^3C may influence tumorigenesis through distinct mechanisms, such as regulation of protein synthesis in metabolic pathways, cell cycle control, and immune evasion-processes central to HCC pathogenesis.

Recent studies have implicated m^3C methylation in tumor development, influencing proliferation, invasion, and metastasis by regulating tumor-related gene expression[21,22]. However, research on m^3C is still in its early stages, and its role in tumors is context-dependent, functioning as a "double-edged sword" across cancer types[23,24]. For example, METTL6 promotes HCC cell proliferation by stabilizing $tRNA^{Met}$, while METTL8 functions as a tumor suppressor in several malignancies. The specific roles of m^3C and its key regulators in HCC-whether oncogenic or tumor-suppressive-remain unclear, as do their associations with clinicopathological features. Moreover, most studies have examined only one or two m^3C regulators in isolation, neglecting their potential coordinated interactions, despite evidence that antitumor effects often rely on the interplay among multiple regulators. A comprehensive understanding of multi-regulator

m^3C-mediated tumor invasion could provide deeper insights into cancer immune regulation and reveal promising therapeutic targets for HCC.

Bioinformatics approaches now enable comprehensive analyses of m^3C regulators and tumor characteristics[25,26]. Our study integrated relevant data from The Cancer Genome Atlas (TCGA) and Gene Expression Omnibus (GEO) to systematically assess m^3C modification patterns in HCC. We examined genetic variations and gene expression of m^3C methylation regulators, identified abnormally expressed regulators, and determined core and characteristic genes predictive of HCC prognosis through protein interaction analyses. Furthermore, by building a scoring system based on the m^3C modification model, we evaluated patient prognosis according to m^3C scores and HCC subtypes. Importantly, our findings reveal a role for m^3C modification in promoting HCC progression and suggest a promising target for prognostic prediction and therapeutic intervention.

METHODS

Cell culture and clinical samples

The HCC cell line HepG2 was cultured in DMEM medium (Gibco, USA) supplemented with 10% fetal bovine serum (FBS; HyClone, USA) and 1% penicillin-streptomycin (HyClone, USA) at 37 °C in a humidified incubator with 5% CO_2. HepG2 cells were transfected with shMETTL2, shMETTL6, shALKBH1, shALKBH3 or a METTL8 overexpression plasmid. Cells transfected with the empty vector served as controls. Transfections were performed using Lipofectamine 3000 reagent (Invitrogen) following the manufacturer's protocol. Forty-eight hours after transfection, cells were harvested to assess overexpression or knockdown efficiency via Quantitative Real-time PCR (qRT-PCR). A total of 16 HCC tissues and the corresponding paracancerous tissues were collected from Xijing Hospital between August 2020 and August 2021. This study was approved by the Medical Ethics Committee of the First Affiliated Hospital of the Air Force Medical University and conducted in accordance with the Declaration of Helsinki and good clinical practice guidelines.

HCC data source and preprocessing

Gene expression data and clinical notes were obtained from 371 HCC patients in The Cancer Genome Atlas Liver Hepatocellular Carcinoma (TCGA-LIHC, downloaded March 2023) and 115 patients from the GEO dataset GSE76427 (downloaded April 2023), totaling 486 patients. Patients with incomplete clinical information (e.g., missing survival time, Tumor Node Metastasis (TNM) stage, or gene expression data) were excluded. Table 1 presents the clinical and pathological characteristics of all 486 patients. RNA sequencing data (Fragments Per Kilobase of exon model per Million mapped fragments, FPKM value) from the TCGA dataset were downloaded from the Genomic Data Commons (GDC, https://portal.gdc.cancer.gov/) and converted to transcripts per million (TPM) values. The "ComBat" algorithm in the sva software package was used to correct batch effects caused by non-biological deviation. Copy number variation (CNV) analysis was performed using somatic mutation data obtained from the TCGA database. All analyses were conducted using R software (version 4.2.2) and R Bioconductor packages.

qRT-PCR

Total mRNA was isolated from liver samples or cells using TRIzol reagent (Merck, 93,289-100 mL) and reverse-transcribed into cDNA with a high-capacity cDNA reverse transcription kit (TAKARA) according to the manufacturer's instructions. mRNA levels were quantified by qRT-PCR using SYBR Green (TAKARA). The relative expression of each cDNA was calculated using the $2^{-\Delta\Delta Ct}$ method with β-actin as the endogenous control. The primer sequences used in this study are shown in Table 2.

Table 1. Clinical and pathological characteristics of HCC patients

Parameters	Values	Total (n = 486) (%)
Age	Median (IQR)	61 (53-70)
	Range (Min, Max)	14-93
	≤ 65	297 (61.1%)
	> 65	188 (38.7%)
	Unknown	1 (0.2%)
Gender	Male	343 (70.6%)
	Female	143 (29.4%)
G stage	0	4 (0.8%)
	1	129 (26.5%)
	2	205 (42.2%)
	3	131 (27.0%)
	4	12 (2.5%)
	Unknown	5 (1.0%)
TNM stage	I	226 (46.5%)
	II	121 (24.9%)
	III	106 (21.8%)
	IV	8 (1.6%)
	Unknown	25 (5.2%)
Clinical T-stage	T1	181 (37.2%)
	T2	94 (19.3%)
	T3	80 (16.5%)
	T4	13 (2.7%)
	Unknown	118 (24.3%)
Clinical N-stage	N0	252 (51.9%)
	N1	4 (0.8%)
	Unknown	230 (47.3%)
Clinical M-stage	M0	266 (54.7%)
	M1	4 (0.8%)
	Unknown	216 (44.5%)

HCC: Hepatocellular carcinoma; TNM: tumor node metastasis.

CCK8 cell proliferation assay

Cells were digested, centrifuged, and resuspended to obtain a single-cell suspension. Cell counts were calculated using a Bio-Rad automatic cell counter. In a 96-well plate, 3,000 cells were seeded per well, with five replicate wells per group. Treated cells were maintained in the 96-well plates, and cell viability was measured daily for five days using the Cell Counting Kit-8 (CCK8, GLPBIO, USA).

Cell wound healing assay (scratch migration test)

Horizontal reference lines were drawn on the back of 6-well plates using a ruler. Cells in the logarithmic growth phase were seeded at 1×10^6 cells/mL (200 μL per well) and cultured overnight. A pipette tip was used to create scratches perpendicular to the reference lines. Cells were washed three times with phosphate buffer saline (PBS) to remove detached cells, then incubated in serum-free medium at 37 °C with 5% CO_2. Images of the wound area were captured at 0 and 24 h.

Unsupervised clustering of m^3C regulators

Six regulators (METTL2A, METTL2B, METTL6, METTL8, ALKBH1, and ALKBH3) were extracted from the TCGA dataset to identify m^3C modification patterns. Interaction information for these regulators was

Table 2. Primer sequences

Primer name	Primer sequence
METTL2A	Forward: 5′-GAAACCTGGCGGGATGATGC-3′
	Reverse: 5′-AGCGTGTCCAGTTCCTCTTGT-3′
METTL2B	Forward: 5′-ACTTCTTCACACAAGAGGAACTG-3′
	Reverse: 5′-TCGGCGGTCCACCAGATT-3′
METTL6	Forward: 5′-CAGGCAAGGATTCTCACCTCT-3′
	Reverse: 5′-TGGTCCAGTGTCTGTCTTTGA-3′
METTL8	Forward: 5′-GGGATCACATGCAGTGGTCTA-3′
	Reverse: 5′-CCCTCAACAGCCAATTACGAT-3′
ALKBH1	Forward: 5′-AAACTTTTCCGCTTCTACCGTC-3′
	Reverse: 5′-TTTGAGTCCATAGGCTTGCCA-3′
ALKBH3	Forward: 5′-TGGGCTGCCCCTGTTAAAAG-3′
	Reverse: 5′-TGTCAATCACTCGTGGCTCAG-3′
β-Actin	Forward: 5′-CATGTACGTTGCTATCCAGGC-3′ Reverse: 5′-CTCCTTAATGTCACGCACGAT-3′
shMETTL2	5′-GCTGAAGATCTGCTGAAAT-3′
shMETTL6	5′-CCAGATGTTCTGCTGATTA-3′
LV-METTL8	Forward: 5′-GGGATCACATGCAGTGGTCTA-3′ Reverse: 5′-CCCTCAACAGCCAATTACGAT-3′
shALKBH1	5′-GGTGAAGATGCTGATGAAT-3′
shALKBH3	5′-GCTGATGTCTGCTGAAGT-3′

obtained from the STRING database (https://string-db.org), and a protein-protein interaction (PPI) network was constructed based on expression relationships. Unsupervised clustering was performed on the expression profiles of these six m^3C regulators to identify distinct modification patterns and classify patients for further analysis. Cluster number and stability were determined using a consensus clustering algorithm. The ConsensusClusterPlus package was used to perform the analysis, repeated 1,000 times to ensure classification stability.

Gene set variation analysis and functional annotation

To investigate differences in biological processes associated with m^3C modification, Gene Set Variation Analysis (GSVA) enrichment analysis was conducted using the "GSVA" R package. GSVA is a nonparametric, unsupervised method typically used to estimate changes in pathway and biological process activity in expression datasets. The "c2. cp. Kegg. v7.4. symbols" gene set was downloaded from the MSigDB database for GSVA analysis. Corrected P values < 0.05 were considered statistically significant. Functional annotation of m^3C-related genes was performed using the clusterProfiler package.

Estimation of tumor microenvironment cell infiltration

The single-sample gene set enrichment analysis (ssGSEA) algorithm was applied to quantify the relative abundance of tumor microenvironment (TME)-infiltrating cells. Gene sets defining each TME immune cell type were obtained from Charoentong *et al.*[27], encompassing human immune cell subtypes such as activated CD4+ and CD8+ T cells, dendritic cells, macrophages, natural killer cells, and regulatory T cells. The ssGSEA enrichment scores represented the relative abundance of each TME-infiltrating cell in each sample.

Identification of differentially expressed genes among m^3C phenotypes

Patients were classified into three m^3C modification modes according to the expression of the six regulators. The empirical Bayesian method in the limma R package was used to identify differentially expressd genes

(DEGs) among these modes. DEGs were considered significant at an adjusted P value < 0.001.

m^{3}C score system

To quantify m^{3}C modification patterns in individual tumors, an m^{3}C scoring system was developed. DEGs from different m^{3}C clusters were normalized, and overlapping genes were identified. Unsupervised clustering was performed on these overlapping DEGs, and a consensus clustering algorithm determined the number and stability of gene groups. Genes significantly associated with prognosis were identified using a univariate Cox regression model, and principal component analysis (PCA) was conducted to construct m^{3}C prognosis-related genes. The m^{3}C score was calculated as: m^{3}C score = Σ (PC1i+PC2i), where i represents the expression level of each m^{3}C prognosis-related gene. Immunophenotypic score (IPS, developed by Charoenton, predict responses to CTLA-4 and PD-L1 antibodies. Correlations between IPS subgroups and m^{3}C molecular groups were evaluated in this study.

Statistical analysis

All statistical analyses were performed using R software (V4.2.2). Repeated one-way ANOVA was used for CCK and wound healing assay results. Categorical variables were analyzed with the chi-square or Fisher's exact test. Gene expression differences between groups were assessed using the Wilcoxon or Kruskal-Wallis test. Pearson or Spearman correlation analyses were conducted to evaluate relationships between variables. A univariate Cox regression model was used to calculate risk ratios for associated genes. Statistical significance was defined as $P < 0.05$.

RESULTS

Expression of m^{3}C-related molecules in HCC and their effects on HCC cell lines

To validate the expression of m^{3}C regulators in clinical liver cancer specimens, we collected tumor and adjacent non-tumor tissues from 16 patients in our hospital. We then measured the relative mRNA levels of m^{3}C regulators. The results showed that, except for METTL8, which was expressed at significantly lower levels in tumor tissues compared with adjacent tissues, the expression of all other m^{3}C regulators was significantly higher in tumor tissues [Figure 1A]. To examine the biological functions of these regulators in HCC, we established lentivirus-based cell lines with knockdown of METTL2, METTL6, ALKBH1, and ALKBH3, as well as overexpression of METTL8, based on their differential expression patterns observed in HCC tissues by qRT-PCR. To assess cell proliferation and migration, we performed CCK8 assays and wound healing (scratch migration) tests. The wound healing assay demonstrated that knockdown of METTL2, METTL6, ALKBH1, and ALKBH3, as well as overexpression of METTL8, significantly reduced the migratory capacity of HCC cells compared with controls [Figure 1B]. Similarly, clone formation assays showed that these manipulations also inhibited HCC cell proliferation [Figure 1C], consistent with the results of the CCK8 assay.

Genetic variation of m^{3}C regulators in HCC

A PPI network of six m^{3}C regulators was established using the STRING database, with different colors indicating their distinct functions [Figure 2A]. CNV analysis revealed noticeable alterations in m^{3}C regulators [Figure 2B] and their chromosomal locations are shown in Figure 2C. To assess whether these genetic mutations influence m^{3}C regulator expression in HCC, we analyzed the mRNA expression levels of regulators in both tumor and adjacent non-tumor samples. Based on database-derived results, differential expression analysis showed that METTL2A, METTL2B, and METTL6 were significantly dysregulated between HCC and paracancerous tissues [Figure 2D]. The distribution of these expression differences is presented in Figure 2E. Mutation frequency analysis demonstrated that four m^{3}C-related genes were mutated in 8 of 371 samples (2.16%), with most m^{3}C regulators exhibiting low mutation rates (< 1%). Only METTL2B showed a relatively higher mutation rate (4/371), indicating that m^{3}C regulators are largely

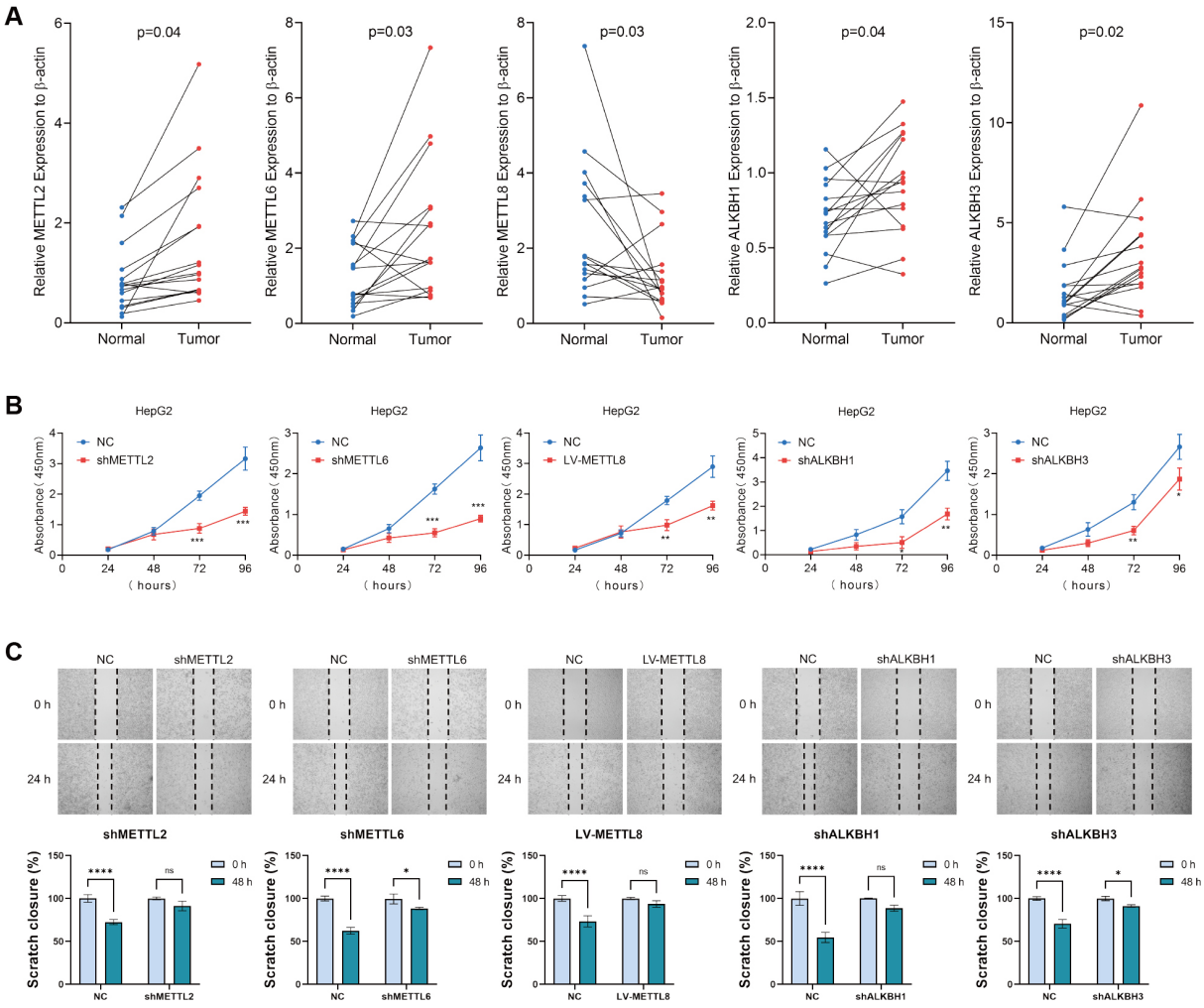


Figure 1. Expression of m^{3}C-related molecules in HCC and their effects on HCC cell lines. (A) Relative mRNA expression levels of six m^{3}C regulators in 16 pairs of HCC and adjacent tissues measured by qRT-PCR; (B) CCK8 assay assessing HCC cell proliferation following m^{3}C regulator knockdown or overexpression; (C) Wound healing assay evaluating changes in cell migration ability after overexpression or downregulation of m^{3}C regulators. (**** $P < 0.0001$, *** $P < 0.001$, ** $P < 0.01$, * $P < 0.05$, ns: not significant, $P > 0.05$). HCC: Hepatocellular carcinoma; m^{3}C: 3-methylcytidine; qRT-PCR: quantitative real-time PCR.

conserved and stable during HCC progression [Figure 2F]. Correlation analysis further revealed significant associations among m^{3}C regulators [Figure 2G]. Survival analyses using TCGA and GEO cohorts indicated that six m^{3}C genes were closely associated with the prognosis of HCC patients [Figure 2H]. A prognostic network was constructed to illustrate the interactions between m^{3}C-related genes and patient outcomes, highlighting the strong relationship between m^{3}C regulators and HCC prognosis [Figure 2I]. Collectively, these results indicate that variations in the expression of m^{3}C regulators may play a critical role in the initiation and progression of HCC.

Determination of the m^{3}C modification model

To explore the role of m^{3}C regulators in prognostic outcomes and clinicopathological characteristics of HCC patients, we used the "CONSENSES Cluster Plus" tool to perform unsupervised clustering of HCC patient data based on m^{3}C methylation regulators. As shown in Figure 3A, the most stable clustering result was obtained when k = 2. Principal component analysis confirmed that this classification method effectively distinguished the two subgroups. Boxplot analysis revealed significant differences in the expression of m^{3}C

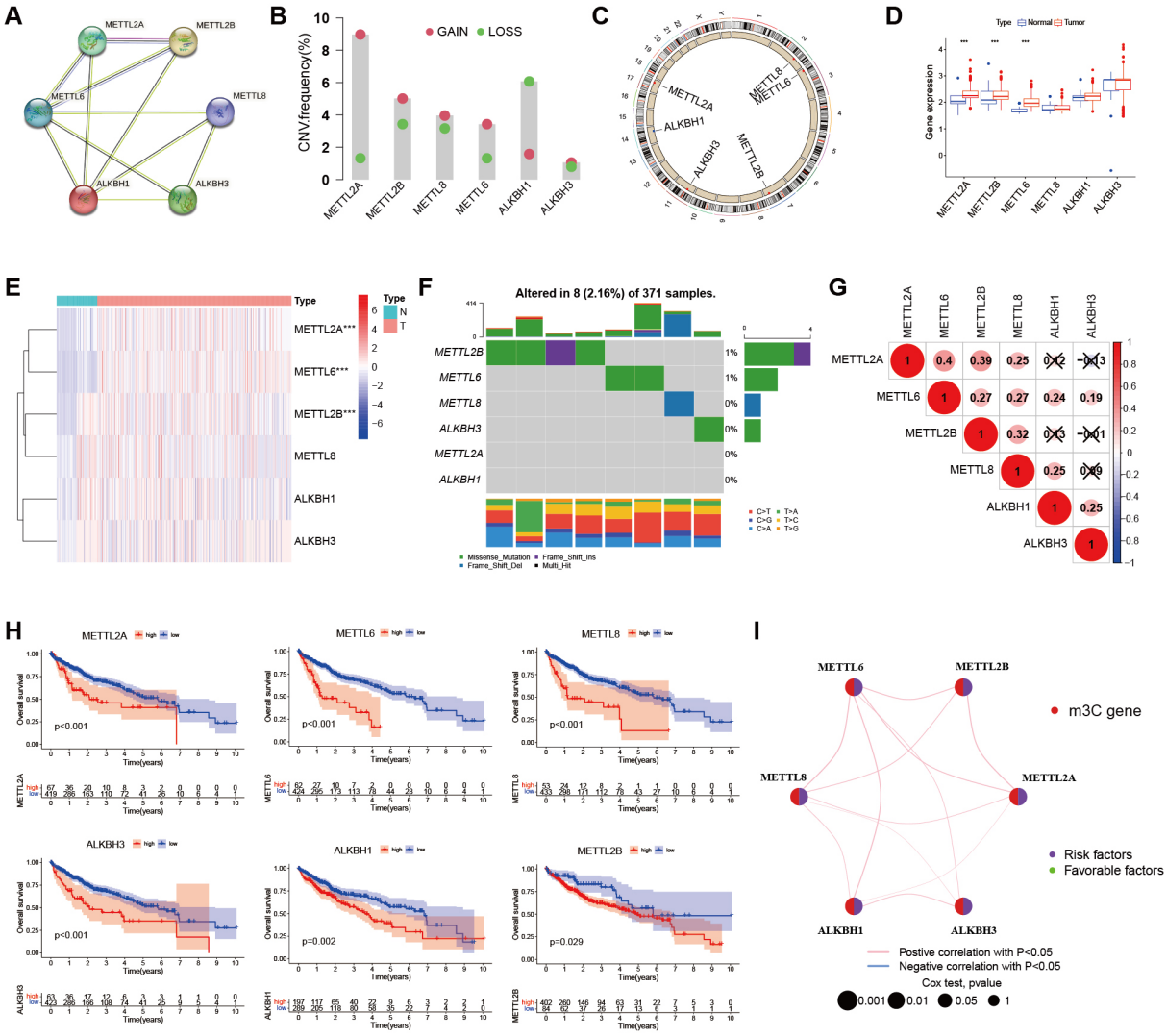


Figure 2. Genetic variation of m^{3}C regulators in liver cancer. (A) PPI network of six m^{3}C regulators constructed using the STRING database; (B) Histogram showing the CNV frequency of the six m^{3}C regulators; (C) Chromosomal locations of CNV alterations in m^{3}C regulators; (D) Boxplot comparing m^{3}C regulator expression levels in normal and cancer samples (*** $P < 0.001$, ** $P < 0.01$, * $P < 0.05$, ns > 0.05); (E) Heatmap of mRNA expression levels of m^{3}C regulators in normal and cancer samples (same significance notation as in D); (F) Mutation frequency of m^{3}C regulators in the TCGA-LIHC cohort (n = 371). The discrepancy with the total cohort size (n = 486) is due to 115 GEO cases lacking somatic mutation data; (G) Pearson correlation analysis of the six m^{3}C methylation regulators in HCC; (H) Prognostic analysis of six m^{3}C regulators using TCGA and GEO databases; (I) Prognostic network showing co-expression relationships among the six m^{3}C regulators. Peripheral nodes represent m^{3}C-related genes, and connections indicate co-expression relationships. Node size reflects the prognostic impact of each regulator. Statistical significance was determined by Cox analysis ($P < 0.001$, $P < 0.01$, $P < 0.05$, $P < 1$). HCC: Hepatocellular carcinoma; m^{3}C: 3-methylcytidine; PPI: protein-protein interaction; CNV: copy number variation; TCGA-LIHC: the cancer genome atlas liver hepatocellular carcinoma; GEO: gene expression omnibus; ns: not significant.

molecules between the two genotypes [Figure 3C]. Heatmap analysis further demonstrated distinct distributions of clinical features across the two m^{3}C subgroups [Figure 3D]. GSVA was then conducted, revealing pathway-level differences between the two groups [Figure 3E]. Finally, differential analysis of immune cell infiltration was performed using the ssGSEA method, and the resulting immune cell scores were compared between groups. The boxplot illustrated differential expression of m^{3}C in relation to specific immune cell populations [Figure 3F].

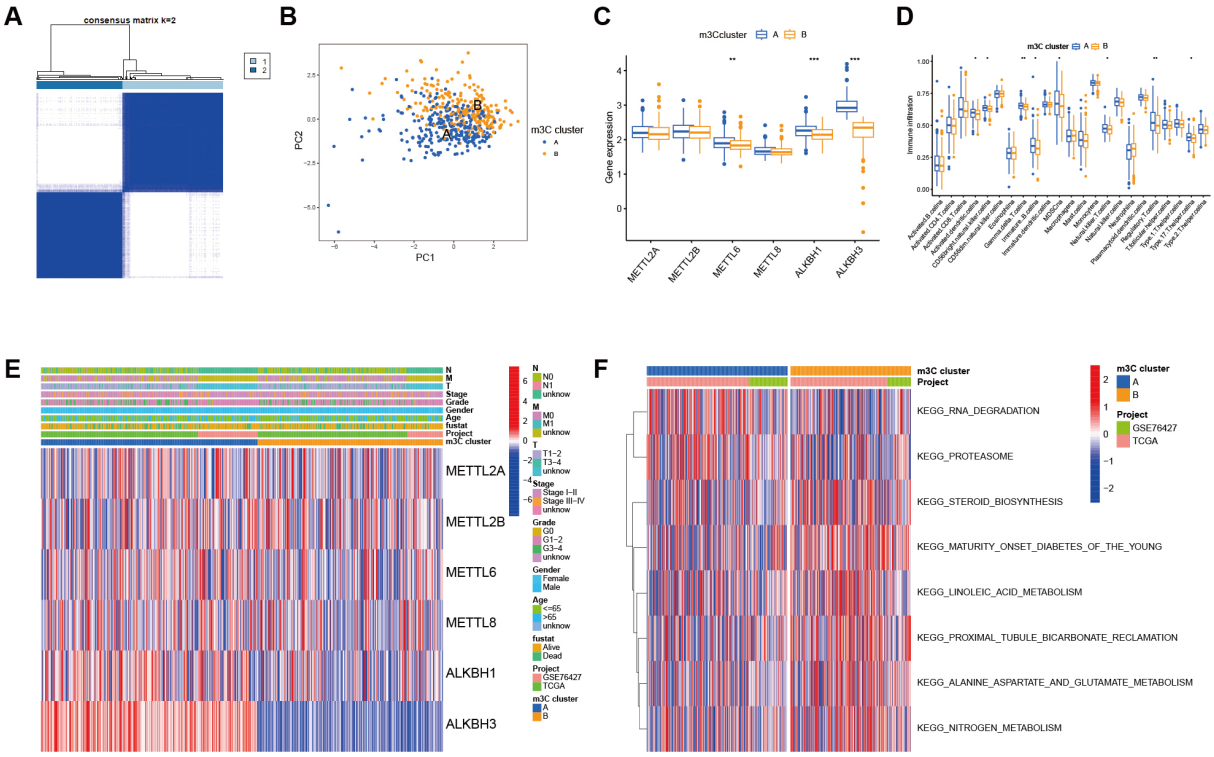


Figure 3. Determination of the m^{3}C modification mode. (A) Two stable subgroups were identified based on the expression similarity of m^{3}C methylation regulators; (B) PCA confirmed that m^{3}C-related genes could distinguish samples between the two subtypes; (C) Boxplot showing differential m^{3}C expression across genotypes; (D) Heatmap illustrating distinct clinical feature distributions between m^{3}C subgroups; (E) GSVA enrichment analysis highlighting biological differences between the two m^{3}C modification modes; (F) ssGSEA analysis showing the abundance of TME-infiltrating cells across the two m^{3}C modification modes.(***$P < 0.001$, **$P < 0.01$, *$P < 0.05$, ns > 0.05). m^{3}C: 3-methylcytidine; PCA: principal component analysis; GSVA: gene set variation analysis; ssGSEA: single-sample gene set enrichment analysis; TME: tumor microenvironment.

Functional annotation of m^{3}C-related genes

Although HCC patients were uniformly clustered using a consensus clustering algorithm, the potential genetic alterations among these m^{3}C-related genes and their functional interactions remain unclear. To address this, we identified the overlapping DEGs between the two m^{3}C clusters. Figure 4A presents the protein-protein interaction network of these DEGs. Interaction data were obtained from the STRING database, and the PPI network was constructed based on expression relationships, with a cut-off interaction score of 0.9 (highest confidence). Kyoto Encyclopedia of Genes and Genomes (KEGG) enrichment analysis revealed that the DEGs were primarily enriched in RNA degradation and endocytosis pathways [Figure 4B]. Gene Ontology (GO) enrichment analysis was then performed to further characterize the functional roles of these DEGs, as shown in the bar and bubble plots. The results [Figure 4C] demonstrated that differential genes were distributed across nearly all cellular functions. In the biological process (BP) category, they were predominantly associated with macroautophagy. In the cellular component (CC) category, enrichment was observed in spliceosomal complexes, which are key structures for pre-mRNA splicing, consistent with m^{3}C's role in post-transcriptional regulation. In the molecular function (MF) category, the DEGs were mainly associated with ubiquitin-like protein binding.

Construction of m^{3}C gene subgroups

We performed survival analysis on individual genes using the database to identify prognosis-related genes. Next, we conducted unsupervised consensus clustering, which classified the patients into three distinct m^{3}C gene subgroups [Figure 5A]. Kaplan-Meier survival curves were then plotted for HCC patients according to

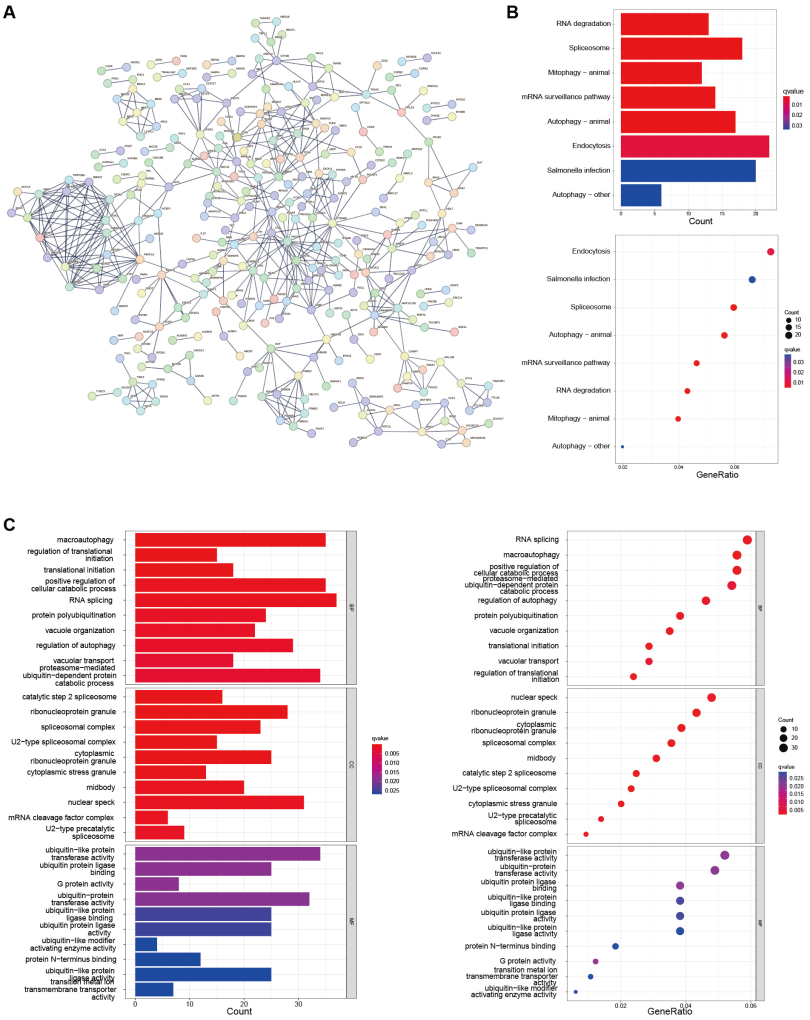


Figure 4. Functional characterization of m^{3}C-related subgroups. (A) A total of 676 DEGs were identified from the intersection of two m^{3}C-defined clusters, and a PPI network was constructed; (B) KEGG enrichment analysis of DEGs, where bar and bubble color depth represents the number of enriched genes; (C) GO enrichment analysis of DEGs across biological process (BP), cellular component (CC), and molecular function (MF) categories. m^{3}C: 3-methylcytidine; PPI: protein-protein interaction; DEGs: differentially expressd genes; KEGG: kyoto encyclopedia of genes and genomes; GO: gene ontology.

genotype [Figure 5B]. The results showed significant differences among the three m^{3}C subgroups, with patients in genotype A having the poorest prognosis ($P < 0.001$). In the box plot, the abscissa represents m^{3}C-related genes and the ordinate indicates gene expression [Figure 5C]. The results demonstrated differential expression of m^{3}C-related molecules across the three subgroups, with most of these genes showing high expression in genotype A. The heatmap based on genotype further illustrated gene expression patterns [Figure 5D], where the abscissa represents samples, the ordinate represents genes, and colors (blue and yellow) indicate subgroup classification. Clinical information was displayed at the top of the heatmap, highlighting distinct clinical characteristics across subgroups. Additionally, immune cell analysis revealed differential expression of m^{3}C-related genes in tumor-infiltrating immune cells [Figure 5E].

Biological characteristics of the m^{3}C score

To quantify the m^{3}C modification pattern based on DEGs, we developed an evaluation system termed the m^{3}C score. As shown in Figure 6A, the m^{3}C score was significantly correlated with both the m^{3}C clusters

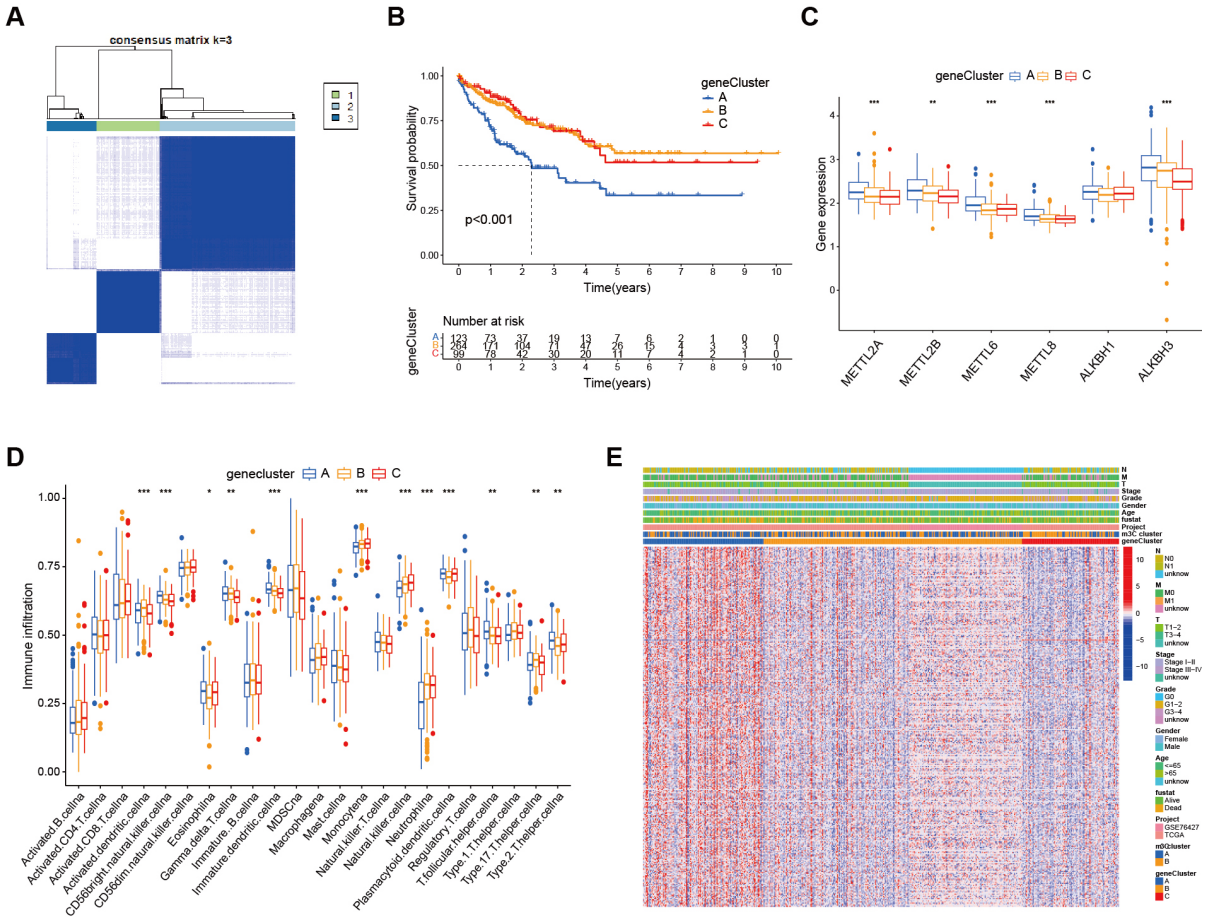


Figure 5. Functional annotation of m^{3}C-related genes. (A) From the DEGs, 330 genes related to HCC prognosis were screened and patients were clustered accordingly, with the most stable results observed when dividing into three groups; (B) Kaplan-Meier survival analysis showed a significant difference between the three genotyping groups; patients in genotype A had a significantly poorest prognosis ($P < 0.01$); (C) Box plots showed differential expression of m^{3}C molecules across the genotypes; (D) Heatmaps based on genotyping revealed distinct clinical characteristics between the groups; (E) ssGSEA analysis demonstrated the abundance of TME infiltrating cells across the two m^{3}C modification subtypes (*** P <0.001, ** P <0.01, * P < 0.05, ns > 0.05). m^{3}C: 3-methylcytidine; DEGs: differentially expressd genes; HCC: hepatocellular carcinoma; ssGSEA: single-sample gene set enrichment analysis; TME: tumor microenvironment; ns: not significant.

and the m^{3}C gene clusters. Survival analysis [Figure 6B] indicated that patients in the high m^{3}C score group had a worse prognosis compared to those in the low score group. Figure 6C presents an alluvial diagram illustrating the distribution of samples across m^{3}C classification, genotype, m^{3}C score, and survival status. Immune correlation analysis further revealed associations between m^{3}C scores and various immune cell populations. As shown in Figure 6D, higher m^{3}C scores were positively correlated with activated CD4 T cells, gamma delta T cells, immature B cells, immature dendritic cells, and several other immune cell types. Conversely, they were negatively correlated with CD56^{dim} natural killer cells, eosinophils, monocytes, neutrophils, and type 17 T helper cells.

The role of m^{3}C score in HCC immunotherapy

We first performed a significance test to evaluate the relationship between the m^{3}C score and Tumor Mutational Burden (TMB) in patients with HCC. Survival analysis showed that patients with lower mutation counts exhibited better survival outcomes compared to those with higher counts (P = 0.047, Figure 7A). Further integration of TMB and m^{3}C scores revealed that patients in the low TMB/low m^{3}C

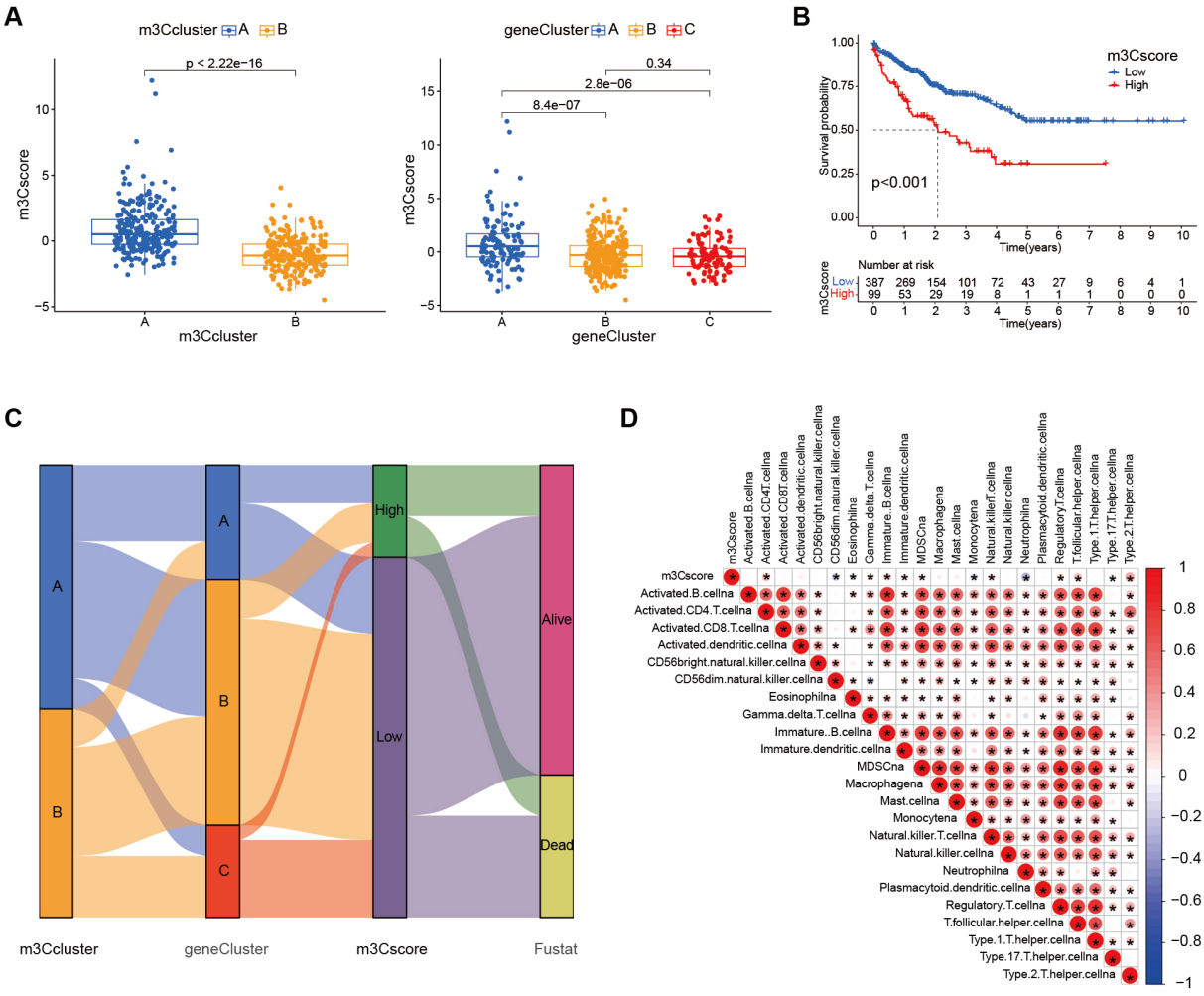


Figure 6. Construction of the m^{3}C scoring system. (A) Box plots showing significant differences in m^{3}C scores between m^{3}C subtypes and genotypes; (B) Kaplan-Meier survival curves demonstrating a significant difference between high and low m^{3}C score groups, with patients in the low-score group exhibiting relatively good prognosis; (C) Alluvial diagram illustrating changes in m^{3}C subtype, genotype, m^{3}C score, and survival status; (D) Correlation between the m^{3}C score and immune cell infiltration as revealed by immune correlation analysis. m^{3}C: 3-methylcytidine.

score group had a significantly better prognosis, whereas those in the high TMB/high m^{3}C score group had a poorer prognosis ($P < 0.001$, Figure 7B). Somatic mutation analysis indicated that TP53 and CTNNB1 mutation rates were generally higher in the high m^{3}C score group compared to the low group [Figure 7C]. Consistently, Figure 7D demonstrates that patients with high m^{3}C scores had lower survival rates than those with low scores. A rank test further confirmed that low m^{3}C scores were associated with prolonged survival [Figure 7E]. Next, we examined the clinical implications of the m^{3}C score. Since HCC is highly immunogenic and tends to respond better to immunotherapy than less immunogenic cancers, early prediction of disease progression and treatment efficacy is crucial for improving patient outcomes. To explore the association between immunotherapy markers and the m^{3}C score, we analyzed PD-L1 and CTLA-4 expression levels. Both were significantly higher in the high m^{3}C score group compared to the low group [Figure 7F]. We also evaluated the relationship between the m^{3}C score and biomarkers of targeted therapy, finding that Kirsten rats sarcoma viral oncogene homolog (KRAS) and V-raf murine sarcoma viral oncogene homolog B1 (BRAF) expression levels were markedly elevated in the high m^{3}C score group [Figure 7G]. The IPS was then employed to assess individual responses to CTLA4 and PD-1 antibodies. We

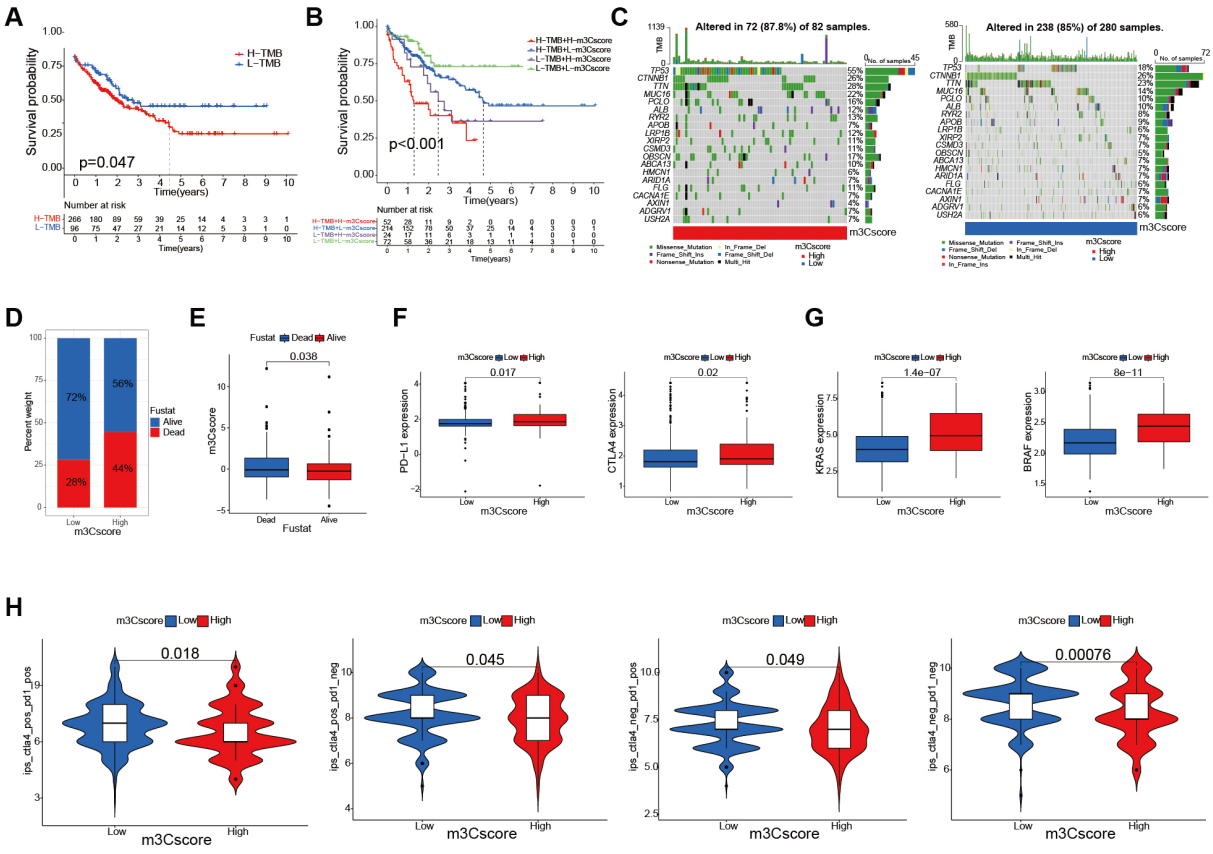


Figure 7. Clinical evaluation of the m^{3}C score. (A) Kaplan-Meier survival curves of patients with high and low TMB (P = 0.047); (B) Survival analysis combining TMB and m^{3}C scores (P = 0.003, log-rank test); (C) Waterfall plot comparing low and high m^{3}C score groups; (D) Survival *vs.* death ratios in high and low m^{3}C score groups; (E) Comparison of m^{3}C scores between surviving and deceased patients (P < 0.001, Wilcoxon test); (F) Relationship between m^{3}C score and immunotherapy markers in HCC patients (P < 0.05, Wilcoxon test); (G) Relationship between m^{3}C score and targeted therapy biomarkers in HCC patients (P < 0.001, Wilcoxon test); (H) Differences in immunophenoscore between m^{3}C score groups (P < 0.0001, Wilcoxon test). m^{3}C: 3-methylcytidine; HCC: hepatocellular carcinoma; TMB: tumor mutation burden.

evaluated how the m^{3}C score influenced IPS and responses to immune checkpoint blockade therapy. As shown in Figure 7H, the median IPS was significantly higher in the low m^{3}C score group across all four subgroups defined by positive or negative CTLA-4 and PD-L1 status. This suggests that, regardless of PD-L1 or CTLA-4 expression, patients with low m^{3}C scores are more likely to benefit from antibody-based immunotherapy.

Clinical evaluation of the m^{3}C score

We further analyzed the relationship between the m^{3}C score and various clinical characteristics of HCC patients. The results showed that across subgroups divided by age, gender, and tumor stage, patients with low m^{3}C scores had better survival outcomes than those with high scores. These findings suggest that the m^{3}C score may serve as a useful prognostic indicator for HCC patients with diverse clinical characteristics [Figure 8A-F].

DISCUSSION

In this study, we performed a comprehensive evaluation of m^{3}C modification patterns in HCC using data from the TCGA and GEO databases. We identified DEGs associated with m^{3}C subtypes, constructed a gene

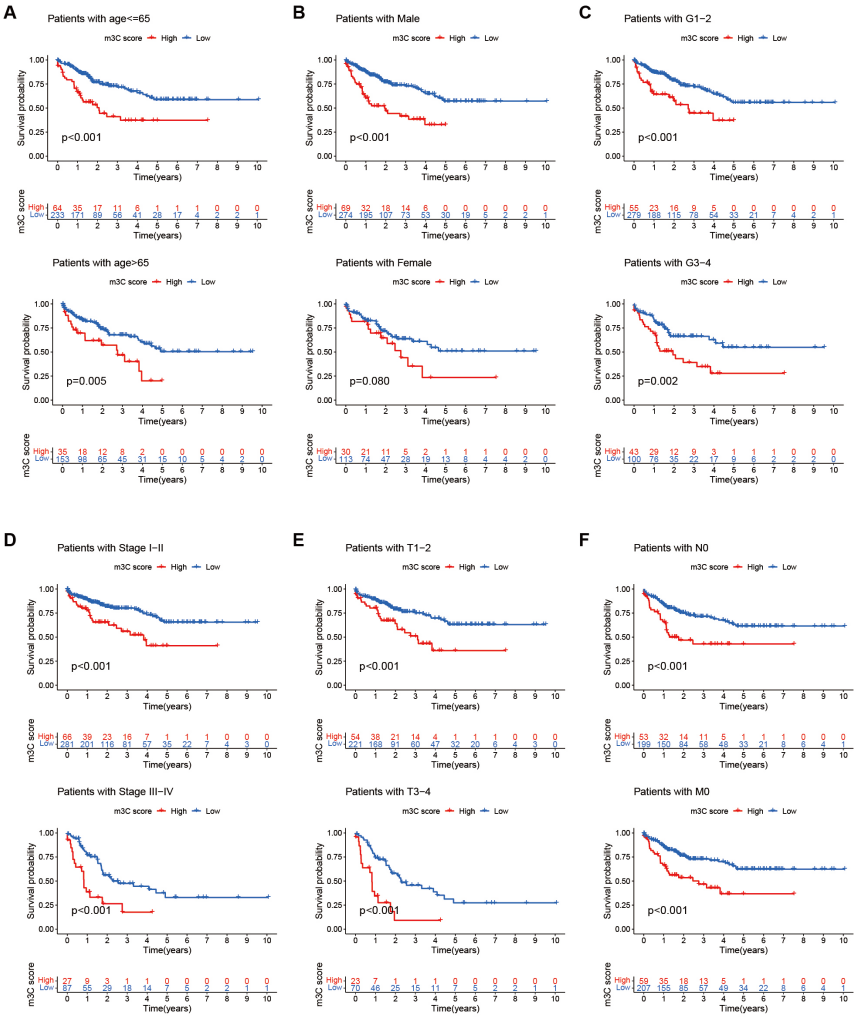


Figure 8. Clinical evaluation of the m^{3}C score. (A-F) Comparison of 5-year survival rates between high and low m^{3}C score groups across different age groups, genders, and tumor T, N, and M stages. Survival analysis revealed that patients with low m^{3}C scores consistently exhibited higher 5-year survival rates than those with high scores in multiple clinical subgroups ($P < 0.05$). m^{3}C: 3-methylcytidine.

cluster model, and developed a quantitative scoring system for m^{3}C modification patterns.

HCC presents significant challenges in early diagnosis and prognosis, making it a major global public health concern[1,2,28,29]. To identify prognostic biomarkers for HCC, it is crucial to elucidate the molecular mechanisms underlying its progression[30-32]. While epigenetic reprogramming is known to play a pivotal role in tumor progression[33-35], the contribution of post-transcriptional mRNA modifications in HCC remains incompletely understood. Unlike m6A-which primarily regulates mRNA splicing and stability-m^{3}C modification is enriched in tRNAs, where it influences stability and translation efficiency. This unique role implicates m^{3}C in tumorigenesis by modulating protein synthesis in key pathways. Recently, m^{3}C has garnered increasing attention[36,37] as one of the most common post-transcriptional base modifications, with important functions reported in several cancers, including breast, pancreatic, and bladder cancers. Importantly, its epigenetic regulation can also shape the tumor immune microenvironment and affect responses to immunotherapy[38-40]. For instance, Wang *et al.* demonstrated that METTL2A is highly amplified in ~7% of invasive breast cancers (BRCA), and its overexpression independently predicts poor

survival by activating DNA synthesis and cell proliferation pathways[40]. Such findings highlight the complexity and heterogeneity of m^{3}C regulators, which may form intricate networks that influence tumor progression.

Ignatova *et al.* reported that METTL6, a tRNA m^{3}C methyltransferase, regulates pluripotency and tumor cell growth: its deletion inhibits HCC cell proliferation, colony formation, and anchorage-independent growth, while reduced expression correlates with improved survival, underscoring its prognostic value[22]. Building on these insights, our literature review identified six key m^{3}C-related genes (METTL2A, METTL2B, METTL6, METTL8, ALKBH1, ALKBH3). Using TCGA and GEO datasets, we found METTL2A, METTL2B, and METTL6 significantly upregulated in HCC tissues. Moreover, expression of all six genes showed a significant negative correlation with survival-suggesting adverse effects on prognosis. Their broad distribution across tumors and interconnections within regulatory networks indicate cooperative functions in cancer progression, as well as potential as therapeutic targets.

To further investigate their role in HCC, we performed consensus clustering based on the expression of 26 m^{3}C regulators, stratifying patients into two subgroups. PCA, GSVA, and immune infiltration analyses revealed distinct m^{3}C methylation landscapes and clinical features. However, survival rates were similar between subgroups-suggesting this classification alone may be insufficient for prognostic modeling. We therefore analyzed DEGs at the intersection of these subgroups, identified prognostic risk genes via univariate Cox regression, and constructed a risk prediction model using consensus clustering. Prognostic analysis confirmed that patients in subgroup A had significantly better outcomes than those in subgroup B, validating the model's predictive accuracy.

Because m^{3}C regulators act mainly as post-transcriptional modifiers, we focused on downstream DEGs, identified prognostic markers, and used them to refine clustering-based stratification. This analysis again revealed substantial differences in patient outcomes, with subgroup A showing superior survival, thereby supporting the utility of our prognostic model in HCC.

Given the heterogeneity of m^{3}C modification patterns across patients, a quantitative scoring system is essential for personalized treatment. We therefore developed the m^{3}C score, which quantifies individual modification patterns. A lower m^{3}C score was associated with better prognosis and correlated with both m^{3}C subtypes and prognosis-related DEG clusters. Immune correlation analysis showed that the score negatively correlated with 10 of 23 immune cell types, suggesting that m^{3}C methylation may promote HCC progression by modulating immune infiltration. Furthermore, associations with clinical characteristics and TNM staging demonstrated the score's independent prognostic value, supporting its application in patient stratification and therapeutic decision making.

Clinically, the m^{3}C score's association with TMB, PD-1, and CTLA4 expression suggests its potential utility in predicting immunotherapy efficacy. Patients with high scores exhibited higher PD-1/CTLA4 expression and IPS, indicating possible responsiveness to immune checkpoint blockade. Nonetheless, this requires validation in independent cohorts with available treatment response data before translation into clinical practice.

Our study has several limitations. First, the clinical validation sample size was small (16 paired samples), limiting the generalizability of m^{3}C regulator expression patterns. Second, bioinformatics analyses relied heavily on TCGA and GEO data; although ComBat correction was applied, batch effects cannot be fully ruled out. Third, functional validation was limited to *in vitro* experiments using HepG2 cells, whereas *in*

vivo studies (e.g., xenograft models) are needed to confirm the role of m^3C regulators in tumor growth. Fourth, the molecular mechanisms by which m^3C modifications affect RNA degradation and endocytosis-such as direct RNA targets of METTL2A/B-remain to be elucidated, requiring methods such as m^3C-seq. Additionally, our immune infiltration analysis was based solely on ssGSEA; future studies incorporating approaches such as CIBERSORT or MCP-counter will be valuable for cross-validation. Finally, the mechanistic links between m^3C modification and immune cell recruitment (e.g., via chemokines such as CXCL9/10 or antigen-presenting molecules) need deeper exploration.

In summary, we investigated the genetic variability and prognostic significance of m^3C regulators in HC, and established a scoring system to predict prognosis and support treatment evaluation. Our findings enhance understanding of m^3C-mediated regulation in HCC and provide a framework for personalized treatment. To strengthen framework applicability, future work will include prospective real-world cohorts, *in vivo* validation, and multi-omics analyses to address current limitations.

DECLARATIONS

Acknowledgments

The authors sincerely thank the TCGA, GEO, and HPA databases for providing access to extensive datasets that supported this study. The authors also thank Liu Hong for valuable advice on the implementation of this study. This work was previously posted as a preprint https://doi.org/10.21203/rs.3.rs-4251076/v1. The present manuscript includes additional analyses and revised interpretations of the data.

Authors' contributions

Conception and design, administrative support: Liu H, and Xiao Li; Hong L, Li X
Collection and assembly of data, data analysis and interpretation: Wei Z, Jun L, Yi W; Zhou W, Lin J, Wang Y
Manuscript writing: Zhou W, Lin J, Wang Y, Fan A
Final approval of the manuscript: Zhou W, Lin J, Wang Y, Fan A, Hong L, Li X

Availability of data and materials

Our data were mined and analyzed using TCGA, GEO, and HPA databases. Further inquiries regarding the original data can be addressed to the corresponding author.

Financial support and sponsorship

This research was funded by the National Natural Science Foundation of China (No.82372693).

Conflicts of interest

All authors declared that there are no conflicts of interest.

Ethical approval and consent to participate

The authors are accountable for all aspects of the work and for ensuring that any questions related to the accuracy or integrity of the study are appropriately addressed. The trial was conducted in accordance with the Declaration of Helsinki (as revised in 2013). The use of human tissue was approved by the Medical Ethics Committee of the First Affiliated Hospital of the Air Force Medical University (#KY20203211-1). Written informed consent was obtained from all participants.

Consent for publication

Not applicable.

Copyright

© The Author(s) 2025.

REFERENCES

1. Qin J, Gong Q, Zhou C, et al. Differential expression pattern of CC chemokine receptor 7 guides precision treatment of hepatocellular carcinoma. *Signal Transduct Target Ther.* 2025;10:229. DOI PubMed PMC
2. Sung H, Ferlay J, Siegel RL, et al. Global cancer statistics 2020: GLOBOCAN estimates of incidence and mortality worldwide for 36 cancers in 185 countries. *CA Cancer J Clin.* 2021;71:209-49. DOI
3. Li M, Cao S, Xu RH. Global trends and epidemiological shifts in gastrointestinal cancers: insights from the past four decades. *Cancer Commun.* 2025;45:774-88. DOI PubMed PMC
4. Donne R, Lujambio A. The liver cancer immune microenvironment: therapeutic implications for hepatocellular carcinoma. *Hepatology.* 2023;77:1773-96. DOI PubMed PMC
5. Thangaraj JL, Coffey M, Lopez E, Kaufman DS. Disruption of TGF-β signaling pathway is required to mediate effective killing of hepatocellular carcinoma by human iPSC-derived NK cells. *Cell Stem Cell.* 2024;31:1327-1343.e5. DOI PubMed PMC
6. Moris D, Martinino A, Schiltz S, et al. Advances in the treatment of hepatocellular carcinoma: an overview of the current and evolving therapeutic landscape for clinicians. *CA Cancer J Clin.* 2025. DOI
7. Sangro B, Sarobe P, Hervás-Stubbs S, Melero I. Advances in immunotherapy for hepatocellular carcinoma. *Nat Rev Gastroenterol Hepatol.* 2021;18:525-43. DOI PubMed PMC
8. Hu Y, Shen ZH. Practice of precision surgery in primary liver cancer. *Hepatobiliary Pancreat Dis Int.* 2021;20:108-9. DOI
9. Haber PK, Castet F, Torres-Martin M, et al. Molecular markers of response to anti-PD1 therapy in advanced hepatocellular carcinoma. *Gastroenterology.* 2023;164:72-88.e18. DOI PubMed PMC
10. Llovet JM, De Baere T, Kulik L, et al. Locoregional therapies in the era of molecular and immune treatments for hepatocellular carcinoma. *Nat Rev Gastroenterol Hepatol.* 2021;18:293-313. DOI
11. Chan YT, Zhang C, Wu J, et al. Biomarkers for diagnosis and therapeutic options in hepatocellular carcinoma. *Mol Cancer.* 2024;23:189. DOI PubMed PMC
12. Schwabe RF, Greten TF. Gut microbiome in HCC - mechanisms, diagnosis and therapy. *J Hepatol.* 2020;72:230-8. DOI PubMed
13. Arvanitakis K, Mitroulis I, Germanidis G. Tumor-associated neutrophils in hepatocellular carcinoma pathogenesis, prognosis, and therapy. *Cancers.* 2021;13:2899. DOI PubMed PMC
14. Suzuki T. The expanding world of tRNA modifications and their disease relevance. *Nat Rev Mol Cell Biol.* 2021;22:375-92. DOI PubMed
15. Zhou JB, Wang ED, Zhou XL. Modifications of the human tRNA anticodon loop and their associations with genetic diseases. *Cell Mol Life Sci.* 2021;78:7087-105. DOI PubMed PMC
16. McCown PJ, Ruszkowska A, Kunkler CN, et al. Naturally occurring modified ribonucleosides. *Wiley Interdiscip Rev RNA.* 2020;11:e1595. DOI PubMed PMC
17. Suzuki T, Yashiro Y, Kikuchi I, et al. Complete chemical structures of human mitochondrial tRNAs. *Nat Commun.* 2020;11:4269. DOI PubMed PMC
18. Huang MH, Peng GX, Mao XL, et al. Molecular basis for human mitochondrial tRNA m^3C modification by alternatively spliced METTL8. *Nucleic Acids Res.* 2022;50:4012-28. DOI PubMed PMC
19. Mao XL, Li ZH, Huang MH, et al. Mutually exclusive substrate selection strategy by human m^3C RNA transferases METTL2A and METTL6. *Nucleic Acids Res.* 2021;49:8309-23. DOI PubMed PMC
20. Cui J, Liu Q, Sendinc E, Shi Y, Gregory RI. Nucleotide resolution profiling of m^3C RNA modification by HAC-seq. *Nucleic Acids Res.* 2021;49:e27. DOI PubMed PMC
21. Schöller E, Marks J, Marchand V, et al. Balancing of mitochondrial translation through METTL8-mediated m^3C modification of mitochondrial tRNAs. *Mol Cell.* 2021;81:4810-4825.e12. DOI PubMed PMC
22. Ignatova VV, Kaiser S, Ho JSY, et al. METTL6 is a tRNA m^3C methyltransferase that regulates pluripotency and tumor cell growth. *Sci Adv.* 2020;6:eaaz4551. DOI
23. Zhang LH, Zhang XY, Hu T, et al. The SUMOylated METTL8 Induces R-loop and Tumorigenesis via m3C. *iScience.* 2020;23:100968. DOI PubMed PMC
24. Feng Q, Wang D, Xue T, et al. The role of RNA modification in hepatocellular carcinoma. *Front Pharmacol.* 2022;13:984453. DOI PubMed PMC
25. Ma CJ, Ding JH, Ye TT, Yuan BF, Feng YQ. AlkB homologue 1 demethylates N^3-methylcytidine in mRNA of mammals. *ACS Chem Biol.* 2019;14:1418-25. DOI
26. Wang X, Han Y, Li J, et al. Multi-omics analysis of copy number variations of RNA regulatory genes in soft tissue sarcoma. *Life Sci.* 2021;265:118734. DOI
27. Charoentong P, Finotello F, Angelova M, et al. Pan-cancer immunogenomic analyses reveal genotype-immunophenotype relationships and predictors of response to checkpoint blockade. *Cell Rep.* 2017;18:248-62. DOI
28. Finn RS, Qin S, Ikeda M, et al; IMbrave150 Investigators. Atezolizumab plus bevacizumab in unresectable hepatocellular carcinoma. *N Engl J Med.* 2020;382:1894-905. DOI

29. Calderaro J, Seraphin TP, Luedde T, Simon TG. Artificial intelligence for the prevention and clinical management of hepatocellular carcinoma. *J Hepatol.* 2022;76:1348-61. DOI PubMed PMC
30. Yang C, Huang X, Li Y, Chen J, Lv Y, Dai S. Prognosis and personalized treatment prediction in TP53-mutant hepatocellular carcinoma: an in silico strategy towards precision oncology. *Brief Bioinform.* 2021;22:bbaa164. DOI
31. Meng Y, Sang Y, Liao J, et al. Single cell transcriptional diversity and intercellular crosstalk of human liver cancer. *Cell Death Dis.* 2022;13:261. DOI PubMed PMC
32. Fujita M, Yamaguchi R, Hasegawa T, et al. Classification of primary liver cancer with immunosuppression mechanisms and correlation with genomic alterations. *EBioMedicine.* 2020;53:102659. DOI PubMed PMC
33. Kan RL, Chen J, Sallam T. Crosstalk between epitranscriptomic and epigenetic mechanisms in gene regulation. *Trends Genet.* 2022;38:182-93. DOI PubMed PMC
34. Wang B, Wang Z, Zhou Z, et al. Inhibition of 6-phosphogluconate dehydrogenase suppresses esophageal squamous cell carcinoma growth and enhances the anti-tumor effects of metformin via the AMPK/mTOR pathway. *Mol Cancer.* 2025;24:97. DOI PubMed PMC
35. Tian Y, Xiao H, Yang Y, et al. Crosstalk between 5-methylcytosine and N^6-methyladenosine machinery defines disease progression, therapeutic response and pharmacogenomic landscape in hepatocellular carcinoma. *Mol Cancer.* 2023;22:5. DOI PubMed PMC
36. Lentini JM, Alsaif HS, Faqeih E, Alkuraya FS, Fu D. DALRD3 encodes a protein mutated in epileptic encephalopathy that targets arginine tRNAs for 3-methylcytosine modification. *Nat Commun.* 2020;11:2510. DOI PubMed PMC
37. Chen R, Zhou J, Liu L, Mao XL, Zhou X, Xie W. Crystal structure of human METTL6, the m^3C methyltransferase. *Commun Biol.* 2021;4:1361. DOI PubMed PMC
38. Lee SA, Lee KH, Kim H, Cho JY. METTL8 mRNA methyltransferase enhances cancer cell migration via direct binding to ARID1A. *Int J Mol Sci.* 2021;22:5432. DOI PubMed PMC
39. Chang Q, Chen P, Yin J, et al. Discovery and validation of bladder cancer related excreted nucleosides biomarkers by dilution approach in cell culture supernatant and urine using UHPLC-MS/MS. *J Proteomics.* 2023;270:104737. DOI
40. Wang S, Li H, Liu J, et al. Integrative analysis of m3C associated genes reveals METTL2A as a potential oncogene in breast cancer. *J Transl Med.* 2022;20:476. DOI PubMed PMC